Added Mass and Aeroelastic Stability of a Flexible Plate Interacting With Mean Flow in a Confined Channel

Rajeev K. Jaiman[1]
Assistant Professor
Department of Mechanical Engineering,
National University of Singapore,
117576 Singapore
e-mail: mperkj@nus.edu.sg

Manoj K. Parmar
Research Assistant
Scientist University of Florida,
Gainesville, FL 32611

Pardha S. Gurugubelli
Graduate Research Assistant
National University of Singapore,
117576 Singapore

This work presents a review and theoretical study of the added-mass and aeroelastic instability exhibited by a linear elastic plate immersed in a mean flow. We first present a combined added-mass result for the model problem with a mean incompressible and compressible flow interacting with an elastic plate. Using the Euler–Bernoulli model for the plate and a 2D *viscous potential flow model, a generalized closed-form expression of added-mass force has been derived for a flexible plate oscillating in fluid. A new compressibility correction factor is introduced in the incompressible added-mass force to account for the compressibility effects. We present a formulation for predicting the critical velocity for the onset of flapping instability. Our proposed new formulation considers tension effects explicitly due to viscous shear stress along the fluid-structure interface. In general, the tension effects are stabilizing in nature and become critical in problems involving low mass ratios. We further study the effects of the mass ratio and channel height on the aeroelastic instability using the linear stability analysis. It is observed that the proximity of the wall parallel to the plate affects the growth rate of the instability, however, these effects are less significant in comparison to the mass ratio or the tension effects in defining the instability. Finally, we conclude this paper with the validation of the theoretical results with experimental data presented in the literature.*
[DOI: 10.1115/1.4025304]

1 Introduction

The determination of added-mass effects has a wide application in the transient analysis of an elastic plate subjected to fluid flow, e.g., flutter analysis [1,2] and vortex-induced vibration [3,4]. The added mass is an inherent characteristic of fluid loading and the understanding of the added-mass will provide the the means for fluid loading to be obtained in the most suitable form for wide ranging applications. Added-mass effects become especially relevant for hydroelastic problems and lightweight structures since the mass of the entrained fluid by the dynamical structure is a significant part of the total mass. The added-mass effect also has an implication in the numerical modeling of the fluid-structure interaction (FSI) and is an important design parameter for the stability and convergence of the underlying coupling scheme; see Refs. [5–10].

The flapping of the elastic plate problem is of interest not only for its prevalence, but also for the simplicity of the problem statement and the richness of the coupled fluid-structure behavior. Consequently, there have been numerous investigations of this problem [2,11–17]. The aeroelastic instability with such a configuration can easily be seen by blowing air over a thin piece of paper and in the waving of flaglike structures. In this paper, we are particularly interested in the very initial stage of instability, where the linearized flow-structure theory is sufficient. The effects of added mass and channel confinement are investigated in the context of the coupled fluid-elastic instability.

The existing knowledge regarding the evaluation of added mass is limited to the elastic plate in incompressible flows. Typically, the importance of the added-mass force is proportional to the fluid to structure density ratio and can justifiably be ignored in compressible flows due to the low density of the gas. However, for lightweight structures, it has significance due to strong unsteady inertial effects. The fluid loading on a flexible plate in an axial flow may be considered as the sum of a noncirculatory part and a circulatory part [2]. The noncirculatory part of the loading involves the added mass, the fluid dynamic damping, and the added stiffening of the plate. The earliest treatment of the flow compressibility effect on an infinite elastic plate motion in Ref. [18] was aimed at the stability analysis of thin panels.

Recently, Brummelen [5] derived an approximate expression for the added-mass of a compressible inviscid flow on an infinite elastic plate for short times. The focus of the work in Ref. [5] was to establish the difference in the compressible and incompressible added-mass force during early times of motion by considering independent sets of equations for the compressible and incompressible flow. For the model elastic plate, the added mass of a compressible flow system is proportional to the length of the time interval, whereas the added mass of an incompressible system asymptotically approaches a constant. This finding has an implication in the design of fluid-structure coupling algorithms and the stability and convergence properties of the subiterations [7–9].

The added-mass force has been extensively studied in multiphase flows. In an incompressible flow, the added-mass force is proportional to the mass of the fluid displaced by the particle times the relative particle acceleration. An important finding is that the added-mass force is independent of the Reynolds number Re see Refs. [19,20]. For a compressible flow, the dependence of the added-mass force on the instantaneous relative acceleration is no longer valid [21–23]. Due to the finite speed of the propagation of sound, the added-mass force depends on the history of the particle relative acceleration and is expressed in an integral form. The integral is expressed as a convolution between the acceleration history and a decaying particle response kernel. The extension of added-mass force in compressible nonlinear regime has been carried out in Ref. [24].

[1]Corresponding author.
Manuscript received May 26, 2013; final manuscript received August 20, 2013; accepted manuscript posted August 28, 2013; published online September 23, 2013. Assoc. Editor: Kenji Takizawa.

The present work builds upon earlier studies of added-mass force in the context of particle interaction with the mean flow [22,23,25]. In the present work, we consider a 2D flexible plate in a rectangular fluid domain. We first perform a theoretical analysis in order to estimate a closed-form for the added-mass force which includes the effects of fluid compressibility, viscosity, and the finite height of the channel. The new generalized formulation reduces to the correct forms in the limiting cases discussed in the literature. A new phenomenon of acoustic stiffening is discussed, which occurs when the spatial wave number of the plate deflection approaches the acoustic wave number in the still fluid. A linear stability analysis is carried out and the effects of the tension, mass ratio, and the height of the channel are discussed. To the best of our knowledge, an exact expression for the added-mass force in compressible flow over an elastic plate has not been discussed thus far in the literature. In addition, the prior work was mainly focused on the flow over an elastic plate in an unconfined domain. The effect of channel height is not discussed in the literature in the context of added-mass effects in the fluid-structure interaction.

The contents of this paper are organized as follows. Section 2 presents the problem statement. In Sec. 3, we derive the fluid loading as a relation between the structural displacement and the corresponding pressure exerted by the linearized fluid on the elastic structure. In Sec. 4, we construct a generalized form of the added mass force, which included the effects of compressibility correction and channel height. Sections 5 and 6 investigate the effects of the tension, channel height, and mass ratio using the linear dispersion analysis.

2 Problem Statement

Many fundamental aspects of the added-mass effect can be derived from a simpler setting of a thin elastic plate oscillating in a mean flow. We consider an elastic plate of length L, width W, and thickness h embedded in a parallel flow with a freestream velocity U_0, as shown in Fig. 1. Let t be the time, x and y be the coordinates in the horizontal and vertical directions, and L and h be the size of the plate in the two directions, as shown in the figure. The solid is modeled as a plate of negligible thickness under the Euler–Bernoulli approximation, i.e., $h/L \ll 1$. Without loss of generality, let the plate be located at the $y=0$ plane. The governing equation per unit length for the vertical displacement of the plate $\alpha(x, t)$ is as follows:

$$\frac{Eh^3}{12(1-\sigma^2)}\alpha_{xxxx} - T\alpha_{xx} + \rho_s h\alpha_{tt} = -\Delta p \tag{1}$$

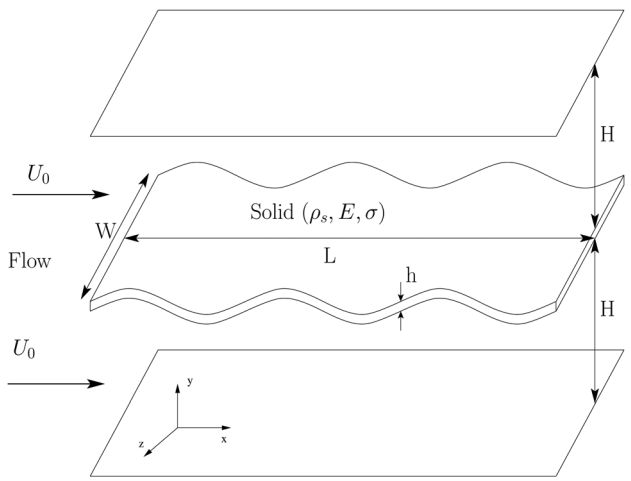

Fig. 1 Depiction of the problem of the two-dimensional elastic plate interacting with the mean flow

where E denotes Young's modulus, ρ_s is the density of the plate, σ is the Poisson ratio of the material, T is the tension acting along axial flow direction, and Δp is the net pressure acting on the plate. We take the plate deflection $\alpha(x, t)$ to be of the harmonic form

$$\alpha(x,t) = \hat{\alpha}e^{ik_x x - i\omega t} \tag{2}$$

where $i = \sqrt{-1}$ and ω and k_x are complex quantities representing the frequency and the wave number in the x-direction, respectively. The preceding relation is a good approximation away from the plate ends. The fluid flow is confined in a distance H above and below the plate, as shown in Fig. 1. We want to find the fluid loading for a small deflection, i.e., $|\dot{\alpha}|/H \ll 1$.

In the absence of any plate deflection, the fluid can be described by a uniform parallel flow with the density, pressure, and velocity in the x-direction as ρ_f, p_0, and U_0, respectively. The assumption of a small plate deflection gives rise to a disturbance flow described by the linearized compressible Navier–Stokes equations as follows:

$$\frac{\partial \rho_f}{\partial t} + U_0\frac{\partial \rho_f}{\partial x} + \rho_f \nabla\cdot\mathbf{u} = 0 \tag{3}$$

$$\rho_f\left(\frac{\partial \mathbf{u}}{\partial t} + U_0\frac{\partial \mathbf{u}}{\partial x}\right) + \nabla p - \mu\Delta\mathbf{u} - \left(\mu_b + \frac{1}{3}\mu\right)\nabla\nabla\cdot\mathbf{u} = 0 \tag{4}$$

where ρ_f, $\mathbf{u} = (u, v)$, and p are perturbations in the fluid density, velocity, and pressure, respectively, with u and v as the velocity components in the x and y directions, μ is the dynamic viscosity, and μ_b is the bulk viscosity of the fluid. In this work, we restrict the size of the disturbance such that the disturbance of the flow can be linearized. In particular, we consider the case of negligibly small perturbations in the temperature field. The undisturbed speed of sound c_0 is used as a closure, where $c_0^2 = p/\rho$. The boundary conditions at the surface of the elastic plate and the horizontal wall at $y = \pm H$ are essentially the no-penetration condition. For small deflections of the elastic plate considered herein, the boundary condition at the top and bottom surface of the elastic plate can be written as

$$v(x,0,t) = \frac{D\alpha(x,t)}{Dt} = \left(\frac{\partial}{\partial t} + U_0\frac{\partial}{\partial x}\right)\alpha(x,t) \tag{5}$$

and at the upper/lower wall we have

$$v(x,\pm H,t) = 0 \tag{6}$$

Because of the inclusion of the viscosity in the governing equations, another set of boundary conditions is needed. Here we will make use of the slip boundary condition on the wall surfaces. This is consistent with the viscous potential theory used in Ref. [5]. The viscous stress parallel to the plate ($y=0$) and the wall surfaces ($y = \pm H$) is taken to be zero, i.e.,

$$\mu\left(\frac{\partial u}{\partial y} + \frac{\partial v}{\partial x}\right) = T = 0$$

Using Eqs. (6) and (5) in the preceding results, we obtain

$$\frac{\partial u}{\partial y}(x,\pm H,t) = 0 \tag{7}$$

$$\frac{\partial u}{\partial y}(x,0,t) = -\frac{\partial}{\partial x}\left(\frac{\partial}{\partial t} + U_0\frac{\partial}{\partial x}\right)\alpha(x,t) \tag{8}$$

As previously described, the viscous shear stress in a potential flow along the flat plate is zero. From the classical Blasius boundary layer theory, it is known that a flat plate experiences a drag force equal to $1.328\ \rho_f U_0^2 \mathrm{Re}^{1/2}$ [26]. This drag force introduces a

tension effect along the plate and the magnitude of this tension along the plate varies as [27]

$$T(x) = C_T \rho_f U_0^2 \mathrm{Re}^{-1/2}\left(1 - \sqrt{\frac{x}{L}}\right) \tag{9}$$

where $C_T = 1.328$ and x is the distance from the leading edge. The preceding equation for the tension force clearly shows that the trailing edge experiences a zero tension, which explains the small amplitude oscillations for the velocity less than the critical velocity [15]. Full body oscillation, however, is observed for the velocity greater than the critical velocity. The proposed model explicitly accounts for the viscous drag effects on the structural side by assuming that the plate is pretensed and the tension is assumed as the average drag force experienced along the plate. Therefore, the average tension can be expressed as

$$\langle T \rangle = \langle C_T \rangle \rho_f U_0^2 \mathrm{Re}^{-1/2} \tag{10}$$

where $\langle C_T \rangle = C_T/3$ denotes the average tension coefficient and $\mathrm{Re} = U_0 L/\nu$ is the Reynolds number.

3 Determination of Fluid Loading

This section is concerned with obtaining a closed form solution for the fluid loading. We can define a scalar potential ϕ and a vector potential $\mathbf{\Psi}$ as follows:

$$u = \nabla\phi + \nabla \times \mathbf{\Psi}, \quad \text{such that} \quad \nabla \cdot \mathbf{\Psi} = 0 \tag{11}$$

For the two-dimensional flow considered here, we can define $\mathbf{\Psi}$ using a scalar potential ψ as follows:

$$\mathbf{\Psi} = \psi \hat{k} \tag{12}$$

where $\hat{k}$ is the unit vector in the z-direction. The velocity components can be expressed as

$$u = \frac{\partial\phi}{\partial x} - \frac{\partial\psi}{\partial y} \quad \text{and} \quad v = \frac{\partial\phi}{\partial y} + \frac{\partial\psi}{\partial x} \tag{13}$$

The perturbation density and pressure can be obtained as follows:

$$p = \rho c_0^2 = \rho_f \left[\left(\lambda + \frac{4}{3}\right)\nu\Delta - \left(\frac{\partial}{\partial t} + U_0\frac{\partial}{\partial x}\right)\right]\phi \tag{14}$$

where $\lambda = \mu_b/\mu$ is the ratio of the bulk to shear viscosity and ν is the kinematic viscosity. It is a simple matter to show that $\phi(x,y,t)$ and $\psi(x,y,t)$ satisfy the following governing equations:

$$\left[1 + \left(\lambda + \frac{4}{3}\right)\frac{i\nu}{c_0^2}\left(\frac{\partial}{\partial t} + U_0\frac{\partial}{\partial x}\right)\right]\Delta\phi = \frac{1}{c_0^2}\left(\frac{\partial}{\partial t} + U_0\frac{\partial}{\partial x}\right)^2\phi \tag{15}$$

$$\Delta\psi = \frac{1}{\nu}\left(\frac{\partial}{\partial t} + U_0\frac{\partial}{\partial x}\right)\psi \tag{16}$$

A general solution for the scalar potentials can be written as

$$\phi(x,y,t) = e^{ik_x x - i\omega t}\left(\beta_1 e^{|k_\phi|y} + \beta_2 e^{-|k_\phi|y}\right) \tag{17}$$

$$\psi(x,y,t) = e^{ik_x x - i\omega t}\left(\gamma_1 e^{|k_\psi|y} + \gamma_2 e^{-|k_\psi|y}\right) \tag{18}$$

where k_ϕ and k_ψ are related to ω and k_x as follows:

$$k_\phi^2 = k_x^2 - \frac{(\omega - U_0 k_x)^2}{c_0^2\left[1 + \left(\lambda + \frac{4}{3}\right)\frac{i\nu}{c_0^2}(\omega - U_0 k_x)\right]} \tag{19}$$

$$k_\psi^2 = k_x^2 + \frac{i}{\nu}(\omega - U_0 k_x) \tag{20}$$

where $|k_\phi|$ and $|k_\psi|$ denotes those values of k_ϕ and k_ψ such that their real parts are non-negative. For complex k_ϕ and k_ψ, the solution given by Eqs. (17) and (18) represents a traveling wave solution consisting of incoming and outgoing waves. For an unconfined domain, i.e., $H \to \infty$, the solution consists of only the outgoing waves. A specific solution can be obtained using the two boundary conditions on the surface of the elastic plate (see Eqs. (5) and (8)).

For the case of a confined channel one can use the four boundary conditions on the surface of the elastic plate and upper wall of the channel, i.e., Eqs. (5)–(8), to obtain the remaining four unknowns: β_1, β_2, γ_1, and γ_2. Thus, we obtain the following expressions for ϕ and ψ for the solution in the upper half domain:

$$\phi(x,y,t) = -i\hat{\alpha}\frac{(\omega - U_0 k_x)}{|k_\phi|}\frac{k_\psi^2 + k_x^2}{k_\psi^2 - k_x^2}\frac{\cosh(|k_\phi|(y-H))}{\sinh(|k_\phi|H)}e^{ik_x x - i\omega t} \tag{21}$$

$$\psi(x,y,t) = 2\hat{\alpha}(\omega - U_0 k_x)\frac{k_x}{k_\psi^2 - k_x^2}\frac{\sinh(|k_\psi|(y-H))}{\sinh(|k_\psi|H)}e^{ik_x x - i\omega t} \tag{22}$$

The solution for the lower domain can be similarly obtained. In general, k_ϕ and k_ψ are complex numbers. Taking the limit of an incompressible flow ($c_0 \to \infty$) and semi-infinite domain ($H \to \infty$), the preceding solution (see Eqs. (21) and (22)) reduces to that represented by Eq. (32) of Ref. [5]. The expression for the pressure perturbation on the surface of the elastic plate, taking into account the effects of compressibility, finite height, and viscosity, can be obtained as follows:

$$p(x,0,t) = -\frac{\rho_f \hat{\alpha}\coth(|k_\phi|H)}{1 + \left(\lambda + \frac{4}{3}\right)\frac{i\nu}{c_0^2}(\omega - U_0 k_x)} \times \left[\frac{(\omega - U_0 k_x)^2}{|k_\phi|} + i2\nu k_x^2\frac{(\omega - U_0 k_x)}{|k_\phi|}\right]e^{ik_x x - i\omega t} \tag{23}$$

In the limit of the incompressible flow, Eq. (19) reduces to $k_\phi^2 = k_x^2$ and we obtain

$$p(x,0,t) = -\rho_f \hat{\alpha}\coth(|k_x|H) \times \left[\frac{(\omega - U_0 k_x)^2}{|k_x|} + i2\nu k_x^2\frac{(\omega - U_0 k_x)}{|k_x|}\right]e^{ik_x x - i\omega t} \tag{24}$$

Further taking the limit of $H \to \infty$, we obtain

$$p(x,0,t) = -\rho_f \hat{\alpha}\left[\frac{(\omega - U_0 k_x)^2}{|k_x|} + i2\nu k_x^2\frac{(\omega - U_0 k_x)}{|k_x|}\right]e^{ik_x x - i\omega t} \tag{25}$$

which is the same as Eq. (33) in Ref. [5]. The net pressure Δp acting on the flexible plate is

$$\Delta p = 2\rho_f \hat{\alpha}\left[\frac{(\omega - U_0 k_x)^2}{|k_x|} + i2\nu k_x^2 \frac{(\omega - U_0 k_x)}{|k_x|}\right] e^{ik_x x - i\omega t} \tag{26}$$

It is clear that the convective and the viscous part in Eq. (25) are proportional to ω, whereas the added-mass part is proportional to ω^2. This implies that the added-mass effect can dominate the effects of convection and viscosity in the limit of $\omega \to \infty$. Furthermore, we observe that the added mass effect in the compressible flow has a localized effect, i.e., the effect of displacement perturbation on the compressible fluid is confined to a region within distance $c_0 t$ of the interface. On the contrary, the effect is global and throughout the entire domain for incompressible flows. This result is consistent with the observation reported in Ref. [5]. In the next section, we present the results of the combined added mass for an oscillating flexible plate.

4 Added-Mass Force

An accelerating body in an inviscid fluid drags a certain amount of fluid due to the no-penetration condition on its surface resulting in the added-mass force. The total force on an oscillating elastic plate under a uniform flow has been derived in the previous section. The added-mass force can be extracted from the total force as the component proportional to the acceleration $\alpha_{tt} = -\omega^2 \hat{\alpha} e^{ik_x x - i\omega t}$. For an oscillating plate under quiescent compressible inviscid fluid, the added-mass force per unit length can be written as

$$F_{\text{am}}(t) = -2\frac{\rho_f W \coth(|k_\phi| H)}{|k_\phi|}\alpha_{tt} \tag{27}$$

where $k_\phi^2 = k_x^2 - k_a^2$ and $k_a = \omega/c_0$ is the acoustic wave number. Using the definition for the added-mass from Ref. [18]

$$m_{\text{am}} = \begin{cases} -2\dfrac{\rho_f W \coth\left(\sqrt{k_x^2 - k_a^2}H\right)}{|k_x|\sqrt{1 - k_a^2/k_x^2}}, & \text{if } k_x > k_a \\ -2\dfrac{\rho_f W \cot\left(\sqrt{k_a^2 - k_x^2}H\right)}{|k_x|\sqrt{k_a^2/k_x^2 - 1}}, & \text{if } k_x < k_a \end{cases} \tag{28}$$

In the limit of a flat plate in the infinite domain, i.e., $H \to \infty$, and an incompressible flow, i.e., $k_a \to 0$, the added-mass tends to the well-known result $m_{\text{am}} = 2\rho_f W/|k_x|$; see Ref. [16]. The finite height effect appears as a multiplicative factor of $\coth(k_x H)$ resulting in

$$m_{\text{am}} = \frac{2\rho_f W \coth(k_x H)}{|k_x|}$$

In Eq. (28), effect of compressibility appears as a correction factor as

$$\xi = \frac{\coth\left(\sqrt{k_x^2 - k_a^2}H\right)}{\sqrt{1 - k_a^2/k_x^2}} \tag{29}$$

For very slow oscillations, i.e., $\omega \to 0$, the incompressible result is again recovered. In an incompressible flow the added-mass force is proportional to the plate acceleration α_{tt}, irrespective of frequency. In a compressible flow, however, the added-mass force and, hence, the added-mass coefficient, is frequency dependent. For $k_a < k_x$ or $\omega < k_x c_0$, compressibility increases the added-mass effect. The compressibility correction factor is shown in Fig. 2. As can be seen, there is a stiffening effect for $\omega \to k_x c_0$. For large frequencies, i.e., $\omega > k_x c_0$, the acoustic wavenumber

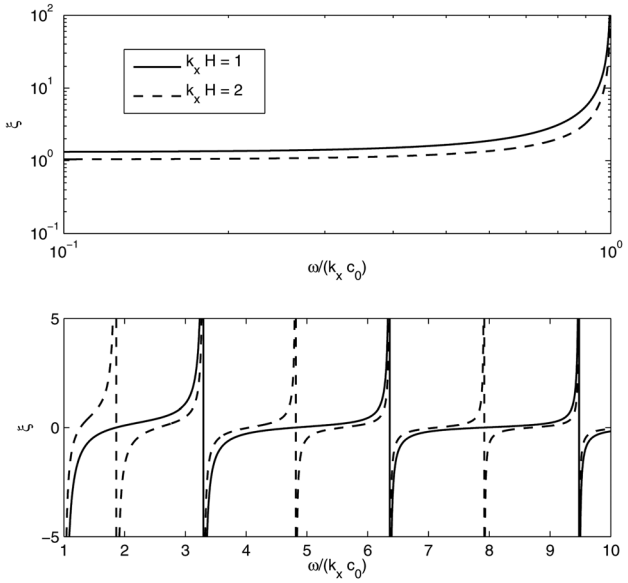

Fig. 2 Compressible correction factor to the added-mass, as given in Eq. (29) for $k_x H = \{1, 2\}$

dominates the plate deflection wavenumber. The effect of the plate deflection is overpowered by the acoustic propagation and in the limit of $k_a/k_x \to \infty$; locally, the problem asymptotes to the behavior of a flat plate vertically oscillating with $k_x = 0$ in a confined channel.

Let us consider the work done by the flat plate surface to increase the kinetic energy of the fluid

$$\frac{dE}{dt} = \int F_{\text{am}} \alpha_t dS = m_{\text{am}} \int \alpha_{tt} \alpha_t dS \tag{30}$$

where E is the kinetic energy, S is the surface bounding the fluid region, and α_t is the velocity of the plate in the normal direction. The added mass m_{am} represents a mass per unit length of the oscillating plate for the rate of change of the kinetic energy in time. When m_{am} is real, the work done is proportional to $\alpha_t \alpha_{tt}$. If the fluid force is given as a complex quantity, its real part is associated with the added mass and the imaginary part is the damping coefficient. For an unsteady problem, the Fourier (Laplace) transform of the unsteady fluid force will have the so-called memory effect, which is related to simply not only the added mass but also to all frequency-dependent forces, i.e., both the added mass and damping effects.

For the case of a flat plate oscillating in a confined domain, we find that m_{am} is always real, i.e., there is no dissipation of energy. In the startup process there is net work done by the plate on the fluid to set the fluid in oscillatory motion, which appears as the kinetic energy of the fluid. After both the plate and fluid system is set into oscillatory motion, there is no net work needed to keep the system in motion. A plate in an infinite domain would, however, lose the energy due to acoustic radiation. Here we draw an analogy with added mass force on an oscillating particle in a compressible inviscid fluid. An oscillating particle in a compressible fluid loses energy to the farfield due to the radiation (see the discussion in Ref. [22]).

To obtain an expression for the nonoscillatory motion, it is useful to cast the preceding equation in the Laplace space. Using $-i\omega = s$, where s is the Laplace variable, Eq. (27) can be rewritten in the Laplace space as

$$\mathcal{L}[F_{\text{am}}] = -\frac{2\rho_f W c_0}{\sqrt{k_x^2 c_0^2 + s^2}}\mathcal{L}[\alpha_{tt}] \tag{31}$$

Defining

$$K(t) = \mathcal{L}^{-1}\left[\frac{2\rho_f W c_0}{\sqrt{k_x^2 c_0^2 + s^2}}\right] = \frac{2\rho_f W}{k_x} J_0(k_x c_0 t) \tag{32}$$

where J_n is the cylindrical Bessel function of the first kind and $K(t)$ is the history kernel relating the acceleration history α_{tt} to the added-mass force as follows:

$$F_{\text{am}}(t) = \int_0^t K(t-\xi)\alpha_{tt} d\xi = \frac{2\rho_f W}{k_x}\int_0^t J_0(k_x c_0(t-\xi))\alpha_{\xi\xi} k_x c_0 d\xi \tag{33}$$

Due to the finite speed of the propagation of sound, the direct proportionality of the added mass force to the acceleration is not valid. The force now depends on acceleration history convoluted with the response kernel $K(t)$. See Ref. [22] for a similar interpretation for an unsteadily moving particle and Ref. [6] in the context of iterative coupling schemes for the fluid-structure interaction. The response kernel for a spherical particle is given by $\exp(-tc_0/a)\cos(tc_0/a)$, where a is the particle radius. The kernel for a spherical particle decays exponentially while the kernel for an oscillating flat plate decays over a longer time due to reflections from the walls of a confined channel.

For a constant acceleration, the force can be shown to be equal to the integration of the kernel. The integration of the kernel $K(t)$ is shown in Fig. 3. Using $J_0(0) = 1$, the early time response $k_x c_0 t \to 0$ can be obtained as

$$\lim_{k_x c_0 t \ll 1} F_{\text{am}}(t) = 2\rho_f W c_0 \int_0^t \alpha_{tt} d\xi \tag{34}$$

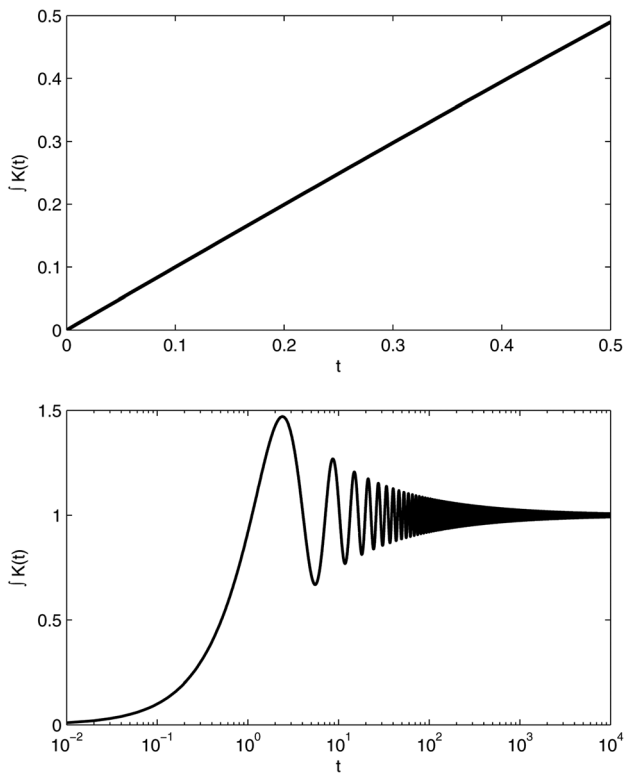

Fig. 3 Integration of kernel $K(t)$ given by Eq. (32), where the early time response (top) and the long time behavior (bottom) are shown

which, for the constant acceleration (α_{tt}), is

$$\lim_{k_x c_0 t \ll 1} F_{\text{am}}(t) = 2\rho_f W c_0 \alpha_{tt} t \tag{35}$$

For the early time the added-mass force in a compressible flow increases linearly with time, as can be seen in Fig. 3 (top). This behavior has also been observed in Refs. [5,6].

Similarly, for a constant acceleration one can obtain a very long time behavior of added-mass as follows:

$$\lim_{k_x c_0 t \gg 1} F_{\text{am}}(t) = 2\rho_f W c_0 \left(\int_0^\infty K(0, k_x c_0(\xi)) d\xi\right)\alpha_{tt} \tag{36}$$

where $k_x c_0 t \gg 1$ can be satisfied if either k_x or c_0 or t is large, i.e.,

$$\lim_{k_x c_0 t \gg 1} F_{\text{am}}(t) = \frac{2\rho_f W}{k_x}\alpha_{tt} \tag{37}$$

Thus, the preceding result is also valid in the incompressible limit, i.e., $c_0 \to \infty$, for all times. As shown in Fig. 3 (bottom), the long time response of the compressible system approaches the incompressible response. Similar behavior was noted in Refs. [22,24] in the context of added mass force on the spherical and cylindrical particles in a compressible flow. In the context of linearized governing equations, at large times the acoustic propagation saturates and the flow field asymptotes to the incompressible one. Thus, the incompressible added mass force is recovered. One can define the added-mass coefficient C_{am} for the incompressible case and the long time behavior of the compressible case as

$$C_{\text{am}} = \frac{m_{\text{am}}}{\rho_f L} \tag{38}$$

which can be further expressed as

$$C_{\text{am}} = \frac{2W}{k_x L} = \frac{\lambda \text{AR}}{n\pi} \tag{39}$$

where n is the mode number, $\lambda = 2\pi/k_x$ denotes the wave length, and $\text{AR} = W/L$ is the aspect ratio. The added mass is thus a function of the nondimensional wave number and is dependent on the flapping mode, which can be interpreted as a layer of fluid with a thickness λ/π around the 2D thin plate case. This is an important difference from the long cylindrical beam problem, in which the added mass is estimated only from the cylinder cross-section. The dependence of the added mass C_{am} diminishes as the flapping mode number n becomes very large. The added mass coefficient increases monotonically as the aspect ratio $\text{AR} = W/L$ increases, especially for plates vibrating in the fundamental mode. The obtained results can also be compared with those of the thin-wing theory [11]. The dependence of the added mass on various modes and aspect ratios can be further studied in a similar manner, as in Ref. [16]. Next, we turn our attention to the linear stability analysis of fluid-elastic flapping modes. Our primary interest is in the onset of instability where the linear theory is sufficient. The questions we want to ask are: (a) what are the factors that lead to the onset of the instability, (b) what is the role of the mass ratio and channel height, and (c) at what flow speed does the plate lose its stability?

5 Stability Analysis

The stability properties of traveling waves propagating in an infinitely long medium in a mean axial flow are now studied. The objective is to predict the existence of instability before performing any detailed analysis and to gain insight into the instability mechanism. In its nondimensional form, the dispersion relation depends on the mass ratio, the nondimensional mean flow

velocity, and the nondimensional channel height. One may classify two cases of wave instability, depending on the long time impulse response of the plate. If the exponentially growing wave packet is advected by the flow, the instability is said to be convective. Conversely, if it grows in place, so that the entire space is ultimately dominated by the instability, the latter is referred to as absolute. The concepts of convective and absolute instabilities, and the underlying theory, have initially been introduced in the domain of plasma physics and successfully applied in the particular domain of fluid-structure interaction [28]. Introducing the Fourier transform in space and time

$$\hat{\alpha}(k,\omega) = \left(\frac{1}{2\pi}\right)^2 \int_{-\infty}^{\infty}\int_{-\infty}^{\infty} \alpha(x,t) e^{i\omega t} e^{-ik_x x} dt dx \tag{40}$$

a dispersion relation for the full system can be derived from the governing equation (see Eq. (1)), the deflection relation (see Eq. (2)), and the solution for fluid loading (see Eq. (23)) as follows:

$$\mathcal{D}(k_x,\omega) = \frac{Eh^3}{12(1-\sigma^2)}k_x^4 - \rho_s h\omega^2 + \langle C_T\rangle \rho_f U_0^2 \mathrm{Re}^{-1/2} k_x^2 - 2\frac{\rho_f \coth(|k_\phi|H)}{1+\left(\lambda+\frac{4}{3}\right)\frac{i\nu}{c_0^2}(\omega - U_0 k_x)} \times \left[\frac{(\omega - U_0 k_x)^2}{|k_\phi|} + i2\nu k_x^2 \frac{(\omega - U_0 k_x)}{|k_\phi|}\right] \tag{41}$$

The deflection relation amplifies in time for all positive imaginary parts and decays for all negative imaginary parts. The value of the imaginary part of the deflection wave/angular frequency describes the disturbance growth rate in time.

In order to determine the temporal instability of the coupled system, we solve the dispersion relation (see Eq. (41)) for the variable ω for all possible real values of k_x and determine if the relation admits any imaginary values of ω. Therefore, the criterion for the temporal instability is that it admits at least one complex ω for any real value k_x. In order to understand the nature of the disturbance in space, we follow the method presented in Ref. [29]. In space a disturbance can grow in the place where it is introduced or grow by advecting downstream. The former is described as the absolute instability and the latter as the convective instability. Starting with $\mathrm{Im}(\omega)$ large and positive, the motion of the spatial roots of Eq. (41) is followed as $\mathrm{Im}(\omega)$ becomes zero. Absolute instability occurs if two roots originating from different halves of the k-plane coalesce for $\mathrm{Im}(\omega)$. If $\mathrm{Im}(\omega)$ can be reduced to zero without coalescing of the roots, the system is, at worst, convectively unstable.

Before moving further, let us consider the nondimensional form of the dispersion relation (see Eq. (41)). By defining the length and time scales

$$L_{\mathrm{ref}} = L, \quad T_{\mathrm{ref}} = \sqrt{\frac{\rho_f L^5 W}{EI}} \tag{42}$$

one can define the nondimensional quantities as follows:

$$\mu = \frac{\rho_s h}{\rho_f L}, \quad k_x' = k_x L_{\mathrm{ref}}$$
$$\omega' = \omega T_{\mathrm{ref}}, \quad U_0' = U_0 \frac{T_{\mathrm{ref}}}{L_{\mathrm{ref}}} \tag{43}$$
$$c_0' = c_0 \frac{T_{\mathrm{ref}}}{L_{\mathrm{ref}}}, \quad \nu' = \nu \frac{T_{\mathrm{ref}}}{L_{\mathrm{ref}}^2}$$

where the $(\cdot)'$ notation is used for the nondimensional quantities. The nondimensionalized dispersion relation is obtained as follows:

$$\mathcal{D}(k_x,\omega) = k_x^4 - \mu\omega^2 + \langle C_T\rangle U_0^{3/2}\nu^{1/2}k_x^2 - 2\frac{\coth(|k_\phi|H)}{1+\left(\lambda+\frac{4}{3}\right)\frac{i\nu}{c_0^2}(\omega - U_0 k_x)} \times \left[\frac{(\omega - U_0 k_x)^2}{|k_\phi|} + i2\nu k_x^2 \frac{(\omega - U_0 k_x)}{|k_\phi|}\right] \tag{44}$$

In the preceding equation and the remaining equations in this section, the $(\cdot)'$ notation for nondimensional quantities is dropped for brevity. For an incompressible flow, Eq. (44) simplifies to

$$\mathcal{D}(k_x,\omega) = k_x^4 - \mu\omega^2 + (C_T)U_0^{3/2}\nu^{1/2}k_x^2 - 2\coth(|k_x|H)\left[\frac{(\omega - U_0 k_x)^2}{|k_x|} + i2\nu k_x^2 \frac{(\omega - U_0 k_x)}{|k_x|}\right] \tag{45}$$

and for an unconfined flow the preceding dispersion relation further simplifies to

$$\mathcal{D}(k_x,\omega) = k_x^4 - \mu\omega^2 + \langle C_T\rangle U_0^{\frac{3/2}{2}}\nu^{1/2}k_x^2 - 2\left[\frac{(\omega - U_0 k_x)^2}{|k_x|} + i2\nu k_x^2 \frac{(\omega - U_0 k_x)}{|k_x|}\right] \tag{46}$$

which is equivalent to the dispersion relation presented in Ref. [30] when the tension effects are neglected.

By setting the dispersion relation for waves on the complete system $\mathcal{D}(k_x,\omega) = 0$, a second order polynomial in ω will be given by

$$\left(\mu + \frac{2}{|k_x|}\coth(|k_x|H)\right)\omega^2 - 4\frac{U_0 k_x}{|k_x|}\coth(|k_x|H)\omega + 2U_0^2|k_x|\coth(|k_x|H) - \langle C_T\rangle U_0^{3/2}\nu^{1/2}k_x^2 - k_x^4 = 0 \tag{47}$$

The stability approach consists of solving the dispersion relation for the frequency variable ω associated to real values of k. The condition for instability, for at least one real value of k, is that the imaginary part of the one root ω is positive, the amplitude of the associated wave $\exp[i(kx - \omega t)]$ grows exponentially with time, and the system is considered locally unstable. For a given wave number k, the critical frequency satisfies the quadratic eigenvalue (see Eq. (47)), where the discriminant is as follows:

$$d_k = \mu k_x^4 + \langle C_T\rangle U_0^{3/2}\nu^{1/2}\left[\mu k_x^2 + 2k_x\coth(k_x H)\right] + \coth(k_x H)(2k_x^3 - 2\mu k_x U_0^2) \tag{48}$$

Based on the dispersion relation, the instability exists if $d_k < 0$ and the system is neutrally stable if $d_k \geq 0$. A critical dimensionless velocity is defined by solving Eq. (48)

$$2\mu\coth(k_x H)U_{\mathrm{cr}}^2 = \mu k_x^3 + \mu k_x\langle C_T\rangle U_{\mathrm{cr}}^{3/2}\nu^{1/2} + 2\coth(k_x H)\left(\langle C_T\rangle U_{\mathrm{cr}}^{3/2}\nu^{1/2} + k_x^2\right) \tag{49}$$

This shows that it is possible to predict the instabilities of a system of this sort simply by looking at the dispersion properties of waves on the interface. For an incoming flow velocity $U < U_{\mathrm{cr}}$ the system is expected to be stable and for $U > U_{\mathrm{cr}}$ the disturbance grows in time, resulting in an unstable system. In the limit of

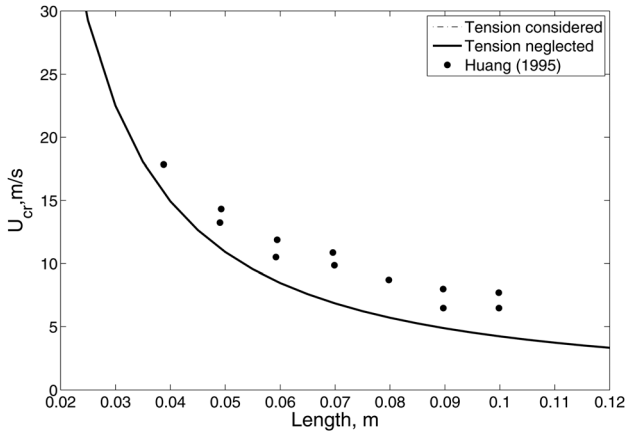

Fig. 4 Comparison between the observed experimental values and the predicted values using Eq. (49). Dots represent Huang's experimental values and the solid and dashed lines coincide in the figure.

the incompressible flow, unbounded domain, and neglecting the tension effects, the dispersion relation reduces to the classical problem extensively analyzed in the literature (see Refs. [28,30–32]).

5.1 Effects of Tension. Figure 4 compares the critical velocity predicted using Eq. (49) for a plate of length L with the experiment conducted by Huang [15] in a wind tunnel. Herein, we consider $k_x = \pi$ for the first fundamental mode. A unique critical flow velocity exists for each specific length of the flexible plate. We observe that the velocity predicted using Eq. (49) is very close to the experimentally observed values. We also observe that the effects of tension due to the viscous shear stress is negligible for air; the critical velocity predicted by considering the tension effects and neglecting tension is nearly identical. In Ref. [15], a simple *ad hoc* procedure based on the growth exponent was used to account for the differences between the experimental results and the formulation given by the potential flow theory.

Figure 5 shows the calculated and the experimental flapping frequency observed by Zhang et al. [33] for a soap film experiment. Earlier theoretical data without tension effects from Ref. [34] are also included in the figure. The experiment uses cylindrical filaments as the flowing soap film in a laminar two-dimensional flow tunnel. The fluid wets the filament, with surface tension forces constraining the filament to lie always in the plane of the film. The length of the filament can be incrementally changed through the holder at the upstream end, which perpendicularly abuts the film. At a fixed flow rate, there exists a critical filament length, below which the filament is stretched straight and aligned with the flow. If the length is sufficiently large, the stable stretched-straight state disappears and only the flapping state remains. The critical frequency predicted by Eq. (46) closely matches with the critical frequency observed in the experiment [33]. We also observe that there is a substantial difference in the predicted values when the tension effects are incorporated into the dispersion relation. The stabilizing effects of tension forces can also be explained as a part of the reason why there was no observable flapping with the water tunnel experiment in Ref. [34]. One can also observe that the frequency of the system decreases as the length of the plate increases, which eventually asymptotes to the flapping frequency of about 50 Hz. This value of the flapping frequency is comparable with the experiment in Ref. [33] for the identical physical parameters. In Ref. [33], a thin vortex street was observed that resulted from a Kelvin–Helmholtz instability. However, the resulting vortical field does not develop eddies of a size comparable to the flapping. Instead, due to the traveling wave and the inextensibility of the plate, the free end executes a figure-eight trajectory.

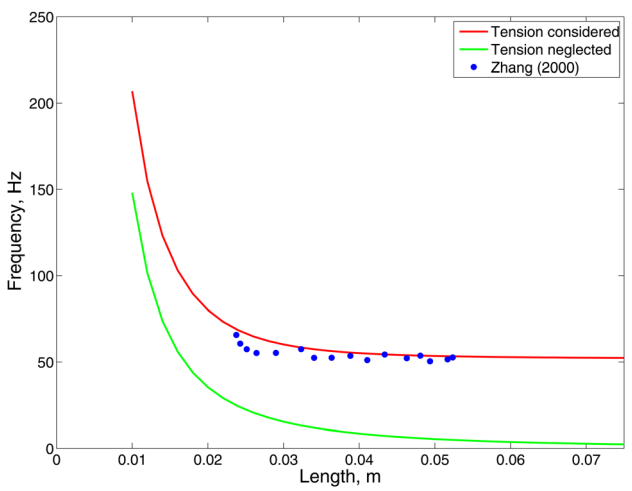

Fig. 5 Comparison between the observed experimental values and the predicted values using Eq. (45)

5.2 Effects of Mass Ratio. As we know, the mass ratio determines which physics dominates the coupled dynamics of the fluid-structure system. In particular, for $\mu \ll 1$ the coupled fluid-structure dynamics is dominated by the fluid inertia and *vice versa* for $\mu \gg 1$, i.e., the structural dynamics dominates the coupled dynamics. Figure 6 shows the effect of the mass ratio on the temporal growth rate of the instability at various mass density ratios μ. Because our aim is to understand effects of the mass ratio on the stability, the dispersion relation is simplified by neglecting the tension effects and the flow domain is assumed to be unbounded. We observe that as the mass ratio increases, the disturbance grows at a faster rate. A similar transient response of the flexible baffle was observed in the fully-coupled fluid-structure simulations for varying mass ratios [7]. As the mass ratio increases, the growth rate of the tip displacement increases in a given time interval for the identical conditions.

Figure 7 describes the spatial instability of the dispersion relation for different values of the mass density ratio. This plot is

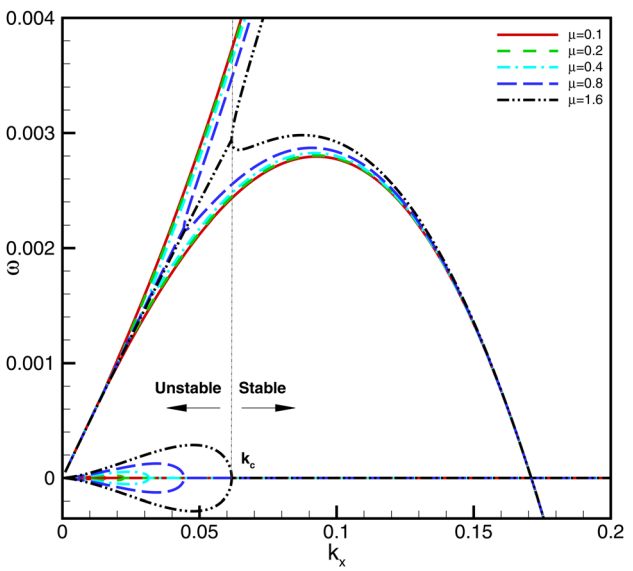

Fig. 6 Effects of the mass ratio μ on the instability growth rate, where $H = \infty$ and $U_0 = 0.05$. For $\mu = 1.6$, the stability boundaries are shown.

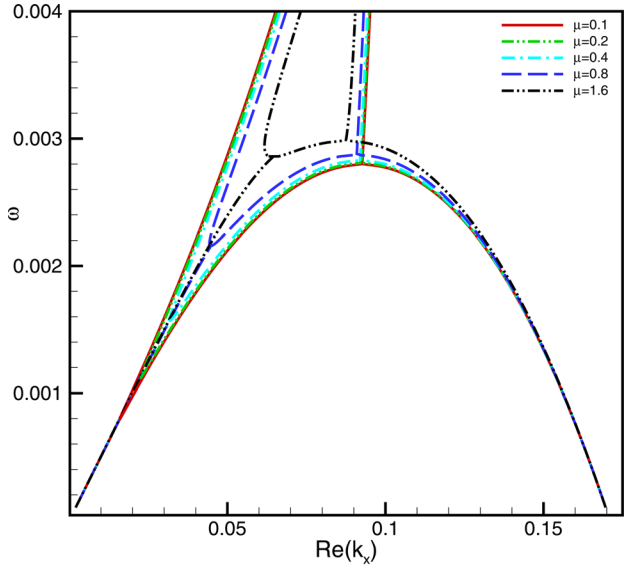

Fig. 7 (*a*) Effects of the mass ratio μ on the convective growth rate of the instability, where $H = \infty$ and $U_0 = 0.05$. The solutions $k_x(\omega)$ of $\mathcal{D}(k_x,\omega) = 0$ are plotted for real positive ω. (*b*) The spatial dispersion diagram for $\mu = 0.8$ and $U_0 = 0.05$. The dashed line denotes the complex modes and the solid line denotes the neutral modes.

created by assuming real values of the angular frequency ω and calculating the complex wave numbers k_x for each of these wave numbers by solving the dispersion relation. The slope of the contours $\partial\omega/\partial k_x$ describes the group velocity of the disturbance (i.e., the advection behavior of the disturbance). The group velocity is the velocity of the energy propagation of fluid-elastic waves and it loses its meaning for the unstable waves. From Fig. 7, we observe that the group velocity of the disturbance is approximately similar for all of the mass ratios. By increasing the mass ratio, the frequency range increases, over which the plate is convectively unstable.

5.3 Effects of Channel Height. This section investigates the effect of the channel height on the aeroelastic instability. In order to understand the effects of the channel height on the stability, the stabilizing effects of tension are neglected. Figure 8 shows the U_{cr} versus μ for different values of the nondimensional channel height H. We observe that with an increase in the finite height H, there is an increase in the value of the critical velocity U_{cr} at a given mass ratio μ. This behavior can be explained with the aid of added mass effects. As the height or channel confinement increases, the added mass force acting on the plate reduces as a multiplier function of $\coth(k_x H)$ (see Eq. (28)). In other words, the more the plate is confined, the larger the added mass. Hence, the smaller the critical value of the velocity for a given mass ratio μ. However, for a very small confinement one may also wonder whether the viscosity has a role on the critical instability limits. Due to the viscous drag of both parallel walls, it may be necessary to consider a boundary layer of a Poiseuille-type flow.

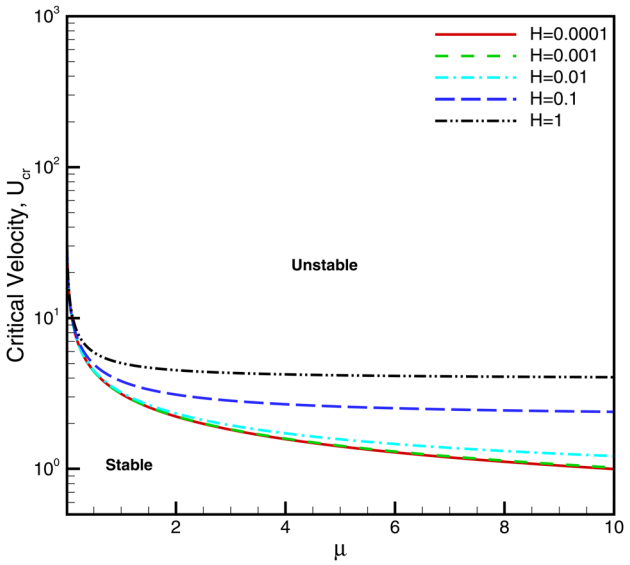

Fig. 8 The stability limit for the flow velocity and critical velocity U_{cr} versus μ for various heights of the channel

Traditionally, the growth of flapping disturbances are associated with the vorticity or curvature effects on the velocity, due to the instability of an interface between two distinct parallel streams (i.e., the Kelvin–Helmholtz instability). However, the instability phenomena reported here are not caused by the vorticity effects. They seem to be associated with the dynamic interaction of the plate with the mean flow, with the major role of the plate tension, elasticity, and the mass ratio. Near the onset point to flapping, the mass of the plate can balance with the surrounding mass of the interacting fluid, while the elastic energy of the plate balances with the kinetic energy of the mean flow.

6 Conclusions

A viscous 2D potential flow analysis for calculating the added mass of a vibrating flexible plate is presented. The combined expression of added mass was derived to account for the effects of compressibility and channel height. The approach assumes an infinite span plate in a viscous potential flow. A new compressibility correction factor was introduced into the generalized form of the added mass for an elastic plate interacting with the mean flow. The effects of the channel height perpendicular to the plate have been investigated. It was found that the added mass effect of the channel confinement modifies the mass ratio and the more the plate is confined, the larger the added mass effects. We have also reported on the flapping instability results of a flexible elastic sheet. We show that the tension force due to the viscous drag can play a significant role in stabilizing inertial effects. A good comparison is reported among the theoretical predictions and experiments.

Further work is now mainly focused on the numerical simulations of a nonlinear fluid-structure analysis. The effects of the mass ratio, tension force, and channel height will be assessed in order to characterize the unsteady added-mass forces and the nonlinear flapping dynamics with vortex shedding and wake vorticity. In future simulations, the critical phase velocity will be determined with the theoretical prediction for a given mean flow speed and structural parameters.

References

[1] Datta, S. and Gottenberg, W., 1975, "Instability of an Elastic Strip Hanging in an Airstream," ASME J. Appl. Mech., **42**, pp. 195–198.

[2] Kornecki, A., Dowell, E. H., and Orien, J., 1976, "On the Aeroelastic Instability of Two-Dimensional Panels in Uniform Incompressible Flow," J. Sound Vib., **47**(2), pp. 163–178.

[3] Blevins, R. D., 1990 *Flow-Induced Vibration*, Van Nostrand Reinhold, New York.

[4] Paidoussis, M. P., 2004, *Fluid-Structure Interactions. Slender Structures and Axial Flow*, Vol. 2, Academic, New York.

[5] Brummelen, E. H., 2009, "Added Mass Effects of Compressible and Incompressible Flows in Fluid-Structure Interaction," ASME J. Appl. Mech., **76**, pp. 173–189.

[6] Brummelen, E. H., 2011, "Partitioned Iterative Solution Methods for Fluid–Structure Interaction," Int. J. Numer. Methods Fluids, **65**, pp. 3–27.

[7] Jaiman, R., Shakib, F., Oakley, O., and Constantinides, Y., 2009, "Fully Coupled Fluid-Structure Interaction for Offshore Applications," Proceedings of the ASME Offshore Mechanics and Arctic Engineering Conference, Honolulu, HI, May 31–June 5, ASME Paper No. OMAE09-79804.

[8] Jaiman, R., 2012, "Advances in ALE Based Fluid-Structure Interaction Modeling for Offshore Engineering Applications," 6th European Congress on Computational Methods in Applied Sciences and Engineering (ECCOMAS 2012), Vienna, Austria, September 10–14.

[9] Forster, C., Wall, W. A., and Ramm, E., 2007, "Artificial Added Mass Instabilities in Sequential Staggered Coupling of Nonlinear Structures and Incompressible Viscous Flows," Comput. Methods Appl. Mech. Eng., **196**, pp. 1278–1293.

[10] Causin, P., Gerbeau, J. F., and Nobile, F., 2005, "Added-Mass Effect in the Design of Partitioned Algorithms for Fluid-Structure Problems," Comput. Methods Appl. Mech. Eng., **194**, pp. 4506–4527.

[11] Jones, R., 1946, "Properties of Low-Aspect Ratio Pointed Wings at Speeds Below and Above the Speed of Sound," NASA Technical Report No. 835.

[12] Dugundji, J., Dowell, E., and Perkin, B., 1963, "Subsonic Flutter of Panels on Continuous Elastic Foundations," AIAA J., **1**, pp. 1146–1154.

[13] Lucey, A. D., 1998, "The Excitation of Waves on a Flexible Panel in a Uniform Flow," Philos. Trans. R. Soc. London, Ser. A, **356**, pp. 2999–3039.

[14] Guo, C. and Paidoussis, M., 2000, "Stability of Rectangular Plates With Free Side-Edges in Two-Dimensional Inviscid Channel Flow," ASME J. Appl. Mech., **67**, pp. 171–176.

[15] Huang, L., 1995, "Flutter of Cantilevered Plates in Axial Flow," J. Fluids Struct., **9**(2), pp. 127–147.

[16] Yadykin, Y., Tenetov, V., and Levin, D., 2003, "The Added Mass of a Flexible Plate Oscillating in a Fluid," J. Fluids Struct., **17**, pp. 115–123.

[17] Shelley, M. J. and Zhang, J., 2011, "Flapping and Bending Bodies Interacting With Fluid Flows," Annu. Rev. Fluid Mech., **43**(1), pp. 449–465.

[18] Minami, H., 1998, "Added Mass of a Membrane Vibrating at Finite Amplitude," J. Fluids Struct., **12**, pp. 919–932.

[19] Mei, R., Lawrence, C. J., and Adrian, R. J., 1991, "Unsteady Drag on a Sphere at Finite Reynolds Number With Small Fluctuations in the Free-Stream Velocity," J. Fluid Mech., **233**, pp. 613–631.

[20] Chang, E. J. and Maxey, M. R., 1995, "Unsteady Flow About a Sphere at Low to Moderate Reynolds Number. Part 2. Accelerated Motion," J. Fluid Mech., **303**, pp. 133–153.

[21] Miles, J. W., 1951, "On Virtual Mass and Transient Motion in Subsonic Compressible Flow," Q. J. Mech. Appl. Math., **4**(4), pp. 388–400.

[22] Parmar, M., Haselbacher, A., and Balachandar, S., 2011, "Generalized Basset-Boussinesq-Oseen Equation for Unsteady Forces on a Sphere in a Compressible Flow," Phys. Rev. Lett., **106**(8), p. 084501.

[23] Parmar, M., Balachandar, S., and Haselbacher, A., 2012, "Equation of Motion for a Sphere in Non-Uniform Compressible Flows," J. Fluid Mech., **699**, pp. 352–375.

[24] Parmar, M., Haselbacher, A., and Balachandar, S., 2008, "On the Unsteady Inviscid Force on Cylinders and Spheres in Subcritical Compressible Flow," Philos. Trans. R. Soc. London, Ser. A, **366**(1873), pp. 2161–2175.

[25] Parmar, M., Balachandar, S., and Haselbacher, A., 2012, "Equation of Motion for a Drop or Bubble in Viscous Compressible Flows," Phys. Fluids, **24**, p. 056103.

[26] Batchelor, G., 1967, *An Introduction to Fluid Dynamics*, Cambridge University Press, Cambridge, UK.

[27] Moretti, P., 2003, "Tension in Fluttering Flags," 10th International Congress on Sound and Vibration, Stockholm, Sweden, July 7–10, pp. 7–10.

[28] Crighton, D. G. and Oswell, J. E., 1991, "Fluid Loading With Mean Flow. I. Response of an Elastic Plate to Localized Excitation," Philos. Trans. R. Soc. London, Ser. A, **335**, pp. 557–592.

[29] Briggs, R. J., 1964, *Electron-Stream Interaction With Plasmas*, MIT, Cambridge, MA.

[30] Peake, N., 2001, "Nonlinear Stability of a Fluid-Loaded Elastic Plate With Mean Flow," J. Fluid Mech., **434**, pp. 101–118.

[31] Landahl, M. T., 1962, "On the Stability of a Laminar Incompressible Boundary Layer Over a Flexible Surface," J. Fluid Mech., **13**(4), pp. 609–632.

[32] Benjamin, T. B., 1963, "The Threefold Classification of Unstable Disturbances in Flexible Surfaces Bounding Inviscid Flows," J. Fluid Mech., **16**(3), pp. 436–450.

[33] Zhang, J., Childress, S., Libchaber, A., and Shelley, M., 2000, "Flexible Filaments in a Flowing Soap Film as a Model for One-Dimensional Flags in a Two-Dimensional Wind," Nature (London), **408**(6814), pp. 835–839.

[34] Shelley, M., Vandenberghe, N., and Zhang, J., 2005, "Heavy Flags Undergo Spontaneous Oscillations in Flowing Water," Phys. Rev. Lett., **94**, p. 094302.